Pacific Northwest
NATIONAL LABORATORY

PNNL-37667 Rev 0
ITSW-RPT-004 Rev 0

FY24 Task 4: Studies of Phosphate and Fluoride Solubility for Dissolution of High Phosphate Tank Waste

April 2025

Trent R Graham
Aurora E Clark
Carolyn I Pearce
Ashley Kennedy
Winnie Liu
Abdullah Ozkanlar
Ege Uyar
Stony T Akins
Daria Boglaienko
Jacob I Morton
Aidan C Henson
Mark E Bowden
Reid A Peterson

U.S. DEPARTMENT of ENERGY

Prepared for the U.S. Department of Energy
under Contract DE-AC05-76RL01830

DISCLAIMER

PACIFIC NORTHWEST NATIONAL LABORATORY
operated by
BATTELLE
for the
UNITED STATES DEPARTMENT OF ENERGY
under Contract DE-AC05-76RL01830

Printed in the United States of America

Available to DOE and DOE contractors from
the Office of Scientific and Technical Information,
P.O. Box 62, Oak Ridge, TN 37831-0062
www.osti.gov
ph: (865) 576-8401
fox: (865) 576-5728
email: reports@osti.gov

Available to the public from the National Technical Information Service
5301 Shawnee Rd., Alexandria, VA 22312
ph: (800) 553-NTIS (6847)
or (703) 605-6000
email: info@ntis.gov
Online ordering: http://www.ntis.gov

PNNL-37667 Rev 0
ITSW-RPT-004 Rev 0

FY24 Task 4: Studies of Phosphate and Fluoride Solubility for Dissolution of High Phosphate Tank Waste

April 2025

Trent R Graham
Aurora E Clark
Carolyn I Pearce
Ashley Kennedy
Winnie Liu
Abdullah Ozkanlar
Ege Uyar
Stony T Akins
Daria Boglaienko
Jacob I Morton
Aidan C Henson
Mark E Bowden
Reid A Peterson

Prepared for
the U.S. Department of Energy
under Contract DE-AC05-76RL01830

Pacific Northwest National Laboratory
Richland, Washington 99354

Acknowledgements

The authors would like to thank Dr. Ming Zhu (DOE-EM) for supporting this work and Amy Westesen for her independent technical review of this report. The authors are extremely grateful to Analytical Chemists Teresa Lemmon and Marie Swita for solution phase analysis in the PNNL Bioscience and Engineering Laboratory (BSEL) Analytical Lab as part of the Chemical and Biological Processing Group in the Energy & Environment Directorate (EED) at Pacific Northwest National Laboratory (PNNL). The authors also thank Rachel Anguish for the quality review of the data package and David MacPherson for his review of this report as well as Matthew Wilburn for his technical editing. Graduate Fellows Ashley Kennedy and Jacob Morton were supported by the Department of Energy Office of Environmental Management – Minority Serving Institutions Partnership Program (EM – MSIPP). PNNL is operated by Battelle for the U.S. Department of Energy under the contract DE-AC05-76RL01830.

Contents

Figures

Tables

1.0 Introduction

Treatment efforts associated with high-level waste (HLW) processing at the Hanford Waste Treatment and Immobilization Plant (WTP) are underway to help accelerate overall mission duration and schedule of the plant. The primary goal of this work is to enable Direct Feed High-Level Waste (DFHLW) by remediating slurry properties in the southeast quadrant of the Hanford tank farms. At present, significant challenges exist relative to the preparation and delivery of feed of sludge directly from waste tanks to the WTP. Eliminating these challenges could remove the need for a standalone pretreatment facility. If the slurry properties are not modified, the throughput for the HLW system will be significantly reduced to accommodate the slurry transport conditions required to achieve overall system throughput.

There is a significant amount of insoluble phosphate and fluoride in southeast quadrant tank waste in the form of natrophosphate ($Na_7FPO_4 \cdot 19H_2O$) (Colburn and Peterson 2021). There has been limited work to define the solubility of natrophosphate and other dominant phases, gibbsite ($Al(OH)_3$) and trisodium phosphate (Na_3PO_4), in the complex tank waste matrix, which also contains sodium salts of hydroxide (OH^-), phosphate (PO_4^{3-}), fluoride (F^-), nitrate (NO_3^-), nitrite (NO_2^-), and aluminate ($Al(OH)_4^-$) (Miller and Britton 2017; Britton 2019a,b; Dembowski et al. 2020). To date, these efforts have not provided sufficient fidelity to (i) determine the conditions required to dissolve these materials and (ii) enable development of operational controls for PO_4^{3-}.

Building on work by Westesen et al. (2023), the current testing seeks to address these knowledge gaps in the solubility of PO_4^{3-} for single- and multi-component systems, with a focus on $Al(OH)_4^-$ in PO_4^{3-}/OH^- mixtures, where predicted values of $Al(OH)_4^-$ solubility have an uncertainty exceeding 50% (Britton 2019b). Carbonate (CO_3^{2-}) is also a major anion, but will be excluded in initial solubility tests, using a CO_3^{2-}-free glovebox, to isolate the effect of PO_4^{3-}. CO_3^{2-} will be added to a subset of compositional conditions to assess its impact on solubility.

In Year 1, the solubility of trisodium phosphate, natrophosphate, and gibbsite in multicomponent aqueous electrolytes containing sodium salts of OH^-, F^-, PO_4^{3-}, NO_3^-, NO_2^-, and $Al(OH)_4^-$, with a subset containing CO_3^{2-}, under various dilution and temperature conditions has been determined. Solubility was determined in a systematic series of solutions, divided into four groups, in which the number of components varied, as described in Section 2.0. This information will be used in Year 2 to determine the temperature and compositional conditions that form a stable solution without gelation or precipitation, with carrier fluid densities suitable for transporting waste under realistic in-tank process conditions.

The longer-term objectives of the work are to determine the optimal temperature and compositional conditions for efficient retrieval of actual waste, using samples from Hanford tank AN-106 as a proof-of-concept. These solutions will potentially be blended with waste from tank AW-105, which contains zirconium and uranium left from fuel decladding. Therefore, clarkeite ($(Na,Ca,Pb)(UO_2)O(OH) \cdot 0\text{-}1H_2O$) and zirconia ($ZrO_2$) will be added to the stable solutions to assess the potential for dissolution and the impact this has on solution stability. This will enable the development of processing schemes that effectively transport these materials without significant downstream solids formation.

2.0 Quality Assurance

This work was performed in accordance with the Pacific Northwest National Laboratory (PNNL) Nuclear Quality Assurance Program (NQAP). The NQAP complies with the United States Department of Energy Order 414.1D, *Quality Assurance,* and 10 CFR 830, Subpart A, *Quality Assurance Requirements*. The NQAP uses NQA-1-2012, *Quality Assurance Requirements for Nuclear Facility Applications,* as its consensus standard and NQA-1-2012, Subpart 4.2.1, as the basis for its graded approach to quality.

The NQAP works in conjunction with PNNL's laboratory-level Quality Management Program, which is based upon the requirements as defined in the United States Department of Energy (DOE) Order 414.1D, *Quality Assurance,* and 10 CFR 830, Subpart A, *Quality Assurance Requirements*.

3.0 Objectives for Solubility Measurements

This section outlines the primary objectives and experimental conditions for determining the solubility of natrophosphate and gibbsite in multicomponent aqueous electrolytes. These electrolytes include sodium salts of OH^-, F^-, PO_4^{3-}, NO^{3-}, NO^{2-}, and $Al(OH)_4^-$, under various dilution and temperature conditions. The key objectives are to measure solubility and identify solubility-limiting phases within these systems, increasing in complexity to a simulant representative of supernatant from tanks AN-101 and AN-106. Experiments were conducted at 20 and 36 °C to assess temperature effects on solubility.

The experiments were divided into four groups: Additional details are provided in the Appendix in tables A1 – A4.

1. Natrophosphate solubility: Solubility measurements of natrophosphate in NaF and Na_3PO_4, with initial sodium concentration increased to a total of 3.8 M using variable amounts of $NaNO_3$, to establish baseline solubility data.
2. Impact of counterion on natrophosphate solubility: Solubility measurements with a fixed total sodium concentration (3.8 M) while varying counterions (OH^-, Cl^-, NO_2^-, NO_3^-, and CO_3^{2-}) to assess their influence on natrophosphate solubility.
3. Natrophosphate and gibbsite solubility in supernatant simulant (Table 1): Measurement of natrophosphate and gibbsite solubility in the simulant, and in simulant supplemented with additional NaOH up to 3.8 M, to investigate interactions between $Al(OH)_4^-$, PO_4^{3-}, and F^-.
4. Natrophosphate and gibbsite solubility upon dilution of the simulant with deionized water: Understanding the impact of dilution on the solubility of natrophosphate and gibbsite by filtering and diluting the supernatant from systems at equilibrium by a factor of 2 or 4.

Table 1 presents the composition of the simulant.

Table 1. 3.8 M Na simulant composition (density = 1.14 g/cm^3).[(a)]

Component	Molecular Weight (g/mole)	Anion / Cation Species	Target Conc. (M)
NaF	41.99	F^-	0.07
Na_3PO_4-12H_2O	380.10	PO_4^{3-}	0.09
$NaNO_2$	69.00	NO_2^-	1.06
$NaNO_3$	84.99	NO_3^-	0.71
NaOH (50% solution, w/w)	40.00	Free OH^-	0.29
Na_2CO_3	106.0	CO_3^{2-}	0.65
$NaAlO_2$	81.97	Al^+	0.09
KCl	74.55	K^+	0.03

(a) Characterization data from Jordan (2022).

4.0 Objectives for Computational Chemistry

The computational chemistry component is designed to complement experimental solubility measurements by offering a detailed perspective on molecular interactions and dynamics within complex aqueous systems. The objective is to incorporate predicted speciation and pre-nucleation behavior – derived from molecular simulations – into statistical and thermodynamic models of solubility across varying solution compositions and temperatures. Initial efforts have focused on developing a robust computational protocol capable of accurately predicting the behavior of sodium phosphate-containing solutions. To aid in the parameterization of classical force field models that capture both intra- and intermolecular interactions, experimentally measured diffusion coefficients, viscosity, and pH have been used – emphasizing the critical role of water polarizability as a solvent medium.

The low solubility of sodium phosphate-containing solutions results in complex aggregation behavior even at low concentrations. To gain a deeper understanding of ion-ion interactions, *ab initio* molecular dynamics (AIMD) simulations have been employed to probe local reactivity. These simulations have revealed the energetic preferences of a wide range of ion-pairing motifs present in solution – many of which closely correspond to those observed in experimentally characterized crystal structures.

The combined classical and *ab initio* computational approach, which combines sampling of the solution ensemble of speciation and aggregation, aims to enhance our understanding of the solubility behavior of trisodium phosphate, natrophosphate, and gibbsite in multicomponent electrolytes under various conditions.

5.0 Materials and Methods

5.1 Reagents

Aqueous solutions for solubility measurements were prepared using nitrogen (N_2) sparged, deionized water (18.2 MΩ·cm). The sodium phosphate dodecahydrate was recrystallized prior to use. All other chemicals were used as received: sodium nitrate ($NaNO_3$, ≥99%, Sigma Aldrich), sodium fluoride (NaF, ≥99%, Sigma Aldrich), sodium phosphate dodecahydrate ($Na_3PO_4 \cdot 12H_2O$, ≥98%, Sigma Aldrich), sodium chloride (NaCl, 99%, Sigma Aldrich), potassium chloride (KCl, ≥99%, Sigma Aldrich), sodium hydroxide (NaOH, 50%, Sigma Aldrich), sodium nitrite ($NaNO_2$, 99%, Sigma Aldrich), sodium carbonate (Na_2CO_3, 99%, Sigma Aldrich), sodium aluminate ($NaAlO_2$, ≥99%, Sigma-Aldrich), and aluminum nitrate nonahydrate ($Al(NO_3)_3 \cdot 9H_2O$, ≥98%, Sigma-Aldrich).

5.2 Gibbsite Synthesis

Gibbsite dissolution can be influenced by particle size and the presence of impurities. Therefore, well-characterized gibbsite nanoparticles of known size and purity will be synthesized following a previously reported method involving neutralization of aqueous aluminum nitrate and subsequent hydrothermal treatment (Zhang et al. 2017). A 0.25 M solution of $Al(NO_3)_3 \cdot 9H_2O$ was adjusted to pH ~5 using a 1 M NaOH solution. The gel-like precipitate was stirred for 1 hour at room temperature, then separated by centrifugation. The precipitate was redispersed in deionized water, washed, and centrifuged through three cycles. After washing, the precipitate was resuspended in 18 MΩ·cm water within a Teflon-lined Parr reaction vessel and heated at 80 °C in an oven with a rotating element (~10 rpm). After 3 days, the synthesized gibbsite nanoplates were collected by centrifugation, washed three times with deionized water, and dried overnight in an oven at 60 °C.

5.3 Natrophosphate Synthesis

Natrophosphate was synthesized by cooling a solution of sodium fluoride and sodium phosphate (Graham et al. 2022). A solution of sodium fluoride was prepared by dissolving 84 g of sodium fluoride (NaF) in 1,000 mL of deionized water (18 MΩ·cm). Separately, a solution of sodium phosphate was prepared by dissolving 164 g of sodium phosphate tribasic ($Na_3PO_4 \cdot 12H_2O$) in 20 g of deionized water. Both solutions were heated to approximately their boiling point, then stirred vigorously for 60 minutes. After removing the stir-bar, the mixture was cooled for 20 hours to ~20 °C and then stored in a refrigerator at 5 °C for 24 hours. The resulting natrophosphate crystals were separated from the solution via vacuum filtration.

5.4 Simulant Preparation

Simulant solutions were prepared in 100-mL volumetric flasks at either 20 or 36 °C by adding reagents, from least to most soluble, in the following order: 30 mL deionized water (18 MΩ·cm), 50% w/w stock solution of sodium hydroxide, sodium fluoride, potassium chloride, sodium nitrite, sodium nitrate, sodium phosphate dodecahydrate, sodium carbonate, and deionized water to bring the solution to final volume. Addition of reagents in this order was required to dissolve the solids. After each reagent addition, the solution was allowed to sit until the reagent fully dissolved. For the reagents added last, the solution was allowed to dissolve for a minimum of 30 minutes before the next reagent was added. Following addition of all reagents, the solution was allowed to stir overnight before use. A number of solutions prepared contained excess

reagents that did not fully dissolve into solution and were challenging to filter, including filtration with a 0.2-µm nylon syringe filter, centrifugation, and vacuum filtration. Final simulants were filtered with a 0.45-µm polypropylene syringe filter at a ratio of 1 filter, heated to either 20 or 36 °C, for every 10 mL of simulant solution. The compositions of all starting solutions were measured by inductively coupled plasma optical emission spectrometry (ICP-OES) and ion chromatography (IC) before use in solubility tests. In the appendix, Table A5 – A7 contain details of these targeted concentration of analytes as well as the experimentally measured concentrations.

5.5 Apparatus for Solubility Experiments

Aqueous solutions were prepared by dissolving the sodium salts in deionized water (18 MΩ·cm) at either 20 or 36 °C. Solubility experiments were initiated from undersaturation conditions by adding gibbsite, such that they were in excess according to literature data, where available (Misra 1970; Delegard et al. 2018). For natrophosphate, iterations were required to add sufficient natrophosphate to exceed the solubility limit. Solubility experiments were conducted in triplicate in an N_2-atmosphere glove box to minimize CO_2 absorption in the alkaline solutions. Teflon reaction vessels were placed inside an aluminum enclosure filled with aluminum beads on a heating stir plate, and the mixtures were stirred at 250 rpm with a magnetic PTFE-lined stir bar. Temperature stability during equilibration was maintained within ± 2 °C, measured using National Institute of Standards and Technology traceable, calibrated thermometers.

5.6 Sampling Solubility Experiments

For sampling, pipette tips were preheated to the solution temperature, and aliquots of ~1.0 mL were collected from the reaction vessels at temperature. These aliquots were quickly filtered through preheated 0.2-µm nylon filters. Sampling was conducted approximately once a day until equilibrium was reached, defined as the plateauing of the concentration values for at least three successive measurements. The reported concentrations are the average of three measurements for each of the triplicate samples (nine measurements total) taken at nominal temperatures of 20 and 40 °C. To determine the actual sampling temperature, calibrations were performed using the known solubility of KNO_3, resulting in temperatures of 20 and 36 °C. All temperatures discussed hereafter are actual sampling temperatures (Zhu et al, 2020).

After sampling, each aliquot was diluted with deionized water, first by 6X, then by 21X, to reach a 168X diluted sample for ICP-OES and IC characterization. Some samples required additional dilutions for IC characterization, with a total dilution factor of either 840X, 1,680X, or 16,800X, to determine Cl^-, PO_4^-, NO_2^-, and NO_3^- concentrations.

After the solubility experiments reached equilibrium, each replicate containing excess natrophosphate was decanted and filtered with a 0.2-µm nylon syringe filter to separate out the undissolved solids from the supernatant. The remaining natrophosphate solids were placed into a sterile cell filter to drip dry and then collected for future analysis. Samples containing excess gibbsite were filtered with a Cole-Parmer polypropylene filter holder containing a 25-mm 0.2-µm nylon filter paper insert. At higher NaOH concentrations, centrifugation was used to separate the solids due to difficulties filtering. The solids were scraped from the filter paper into a weigh boat and allowed to dry before collection for future analysis. All samples of collected supernatant were split into aliquots to be measured for total alkalinity, total carbon, pH, density, and viscosity analysis.

5.7 Solution Phase Analysis

The analytical work was performed in the Bioproducts, Sciences, and Engineering Laboratory Analytical Analysis Center at Pacific Northwest National Laboratory. Aluminum and phosphorous concentrations were determined using a PerkinElmer Avio 550 ICP-OES instrument equipped with a Meinhard nebulizer, a glass cyclonic spray chamber, and a 2.0-mm alumina injector. The instrument was operated with Syngistix software, version 5.5. Calibration standards were prepared from certified sources and verified with an independent set of certified standards. Both calibration and quality control standards were analyzed daily. Samples were diluted in deionized water or dilute nitric acid for Al as necessary to ensure they fell within the calibration range. Samples and standards were measured in triplicate to assess accuracy. Matrix standards of known composition by mass were included with the samples, and the compositions were verified by the analytical method. The experimental setup and analytical methods have inherent uncertainty, and sources of uncertainty were documented and evaluated. Nitrite, nitrate, fluoride and chloride concentrations were measured using a Dionex Reagent Free Ion Chromatography System 5000 (RFICS-5000) with an AS-AP auto-sampler.

A concentration series of aqueous solutions were prepared using Na_3PO_4 and $Na_3PO_4 \cdot 0.167NaOH \cdot 12H_2O$ in an N_2-filled glovebox to determine the concentration-dependent diffusivity of ^{23}Na and ^{31}P with nuclear magnetic resonance (NMR) spectroscopy for benchmarking of force fields used in molecular dynamics simulations.

Pulsed-field gradient stimulated echo ^{23}Na NMR spectra were acquired with the DgcsteSL_cc pulse sequence on an 11.7 T NMR spectrometer equipped with a broadband probe at a temperature of 20 °C. The temperature was calibrated from the 1H chemical shifts of a flame-sealed sample of ethylene glycol. The time domain size was 6,250 complex points, the sweep width was 6,250 Hz, the acquisition time was 1 second, the diffusion gradient pulse length was 4.8 ms, and the diffusion time was 50 ms. A total of 128 transients were acquired with 4 steady state pulses applied prior to the acquisition. The π/2 pulse length was 12.3 µs. Sixteen gradient steps were used, with the gradient levels optimized for each measurement. The diffusion coefficient was calculated from the integrated signal intensity using a single component model, and the gradients were calibrated with the ^{1}H NMR diffusion coefficient of water at a temperature of 25 °C.

Pulsed-field gradient stimulated echo ^{31}P NMR spectra were also obtained using the DgcsteSL_cc pulse sequence on the 11.7 T NMR spectrometer at a calibrated temperature of 20 °C. The time domain size was 26,000 complex points, the sweep width was 52,083 Hz, the acquisition time was 5 seconds, the diffusion gradient pulse length was 5 ms, and the diffusion time was 50 ms. A total of 32 transients were acquired with 16 steady state pulses. The π/2 pulse length was 16.5 µs, and the relaxation delay was 5 seconds. Eighteen gradient steps were used for this experiment, with the gradient levels optimized for each set of conditions. As with ^{23}Na NMR, the diffusion coefficient was calculated from the integrated signal intensity using a single component model and the gradients were calibrated with the ^{1}H NMR diffusion coefficient of water at a temperature of 25 °C.

5.8 Simulations

Classical molecular dynamics (CMD) simulations of phosphate-containing systems are challenging, as standard force fields often overestimate ion-ion attraction, leading to unphysically high aggregation. Previous efforts to parameterize force fields for phosphate in

solution have not resolved this issue. The problem is less severe for protonated phosphate species, which carry lower charge densities. A major limitation lies in the use of nonpolarizable water models, which, although tuned to reproduce bulk water properties such as the dielectric constant (~80 at room temperature), fail to account for reduced permittivity in mixed electrolyte solutions. This reduction arises from the medium's limited polarization in the presence of charged species. Without explicit electronic polarization, nonpolarizable models overestimate Coulombic interactions, leading to exaggerated aggregation – particularly for highly charged ions like phosphate – even at concentrations below their solubility limit.

The electronic continuum correction (ECC) method addresses the overestimation of ion-ion interactions in nonpolarizable force fields by scaling ionic charges to account for the solvent's electronic permittivity. A typical scaling factor of ~0.75 is commonly applied, though it can vary with solution composition and concentration. In this work, we adopted the Madrid force field family as a baseline, as it incorporates ECC-based charge scaling and is parametrized to accurately model electrolyte solution properties. Since the Madrid force field lacks parameters for phosphate, we used the AMBER model, which is known to be compatible with charge scaling. All simulations employed the TIP4P/2005 water model, consistent with the Madrid force field's original parametrization.

Simulation box compositions were determined based on the equilibrium constant (K_b) for phosphate in water, resulting in significant concentrations of PO_4^{3-}, HPO_4^{2-}, and OH^- ions across all cases, with negligible $H_2PO_4^-$ present. System sizes were incrementally increased – from 1,000 to 4,000, then 8,000 and 12,000 water molecules – to assess finite-size effects. Radial distribution function analysis showed that a system with 8,000 water molecules was sufficient to eliminate size-dependent artifacts and reliably capture clustering behavior. For temperature-dependent simulations, the Van't Hoff equation was used to calculate the new K_b values and, subsequently, new concentrations.

Complementing the CMD simulations, *ab initio* simulations were used to study Na binding preferences to phosphate, as well as the energetics of ion-ion interactions. The PBE/DZVP-MOLOPT-SR-GTH density functional and basis were used, as implemented in the CP2K software package. For denticity studies, a 14.5 Å x 14.5 Å x 14.5 Å cubic simulation box containing 100 H_2O and Na_3PO_4 ions (~0.55 m) at 25 °C was employed. For studying sodium phosphate interactions, 200 H_2O and 2 Na_3PO_4 ions (~0.55 m) at 25 °C were examined.

6.0 Solubility Results

The solubility of natrophosphate in multicomponent electrolytes containing $NaNO_3$, NaF, and $Na_3PO_4{\cdot}0.167NaOH{\cdot}12H_2O$ was determined. The experiments were conducted with varying concentrations of NaF and $Na_3PO_4{\cdot}0.167NaOH{\cdot}12H_2O$ and with a total sodium concentration held constant at 3.8 M by addition of $NaNO_3$. NaF concentrations were 0, 0.05, 0.1, and 0.15 M, and $Na_3PO_4{\cdot}0.167NaOH{\cdot}12H_2O$ concentrations were 0.05, 0.1, and 0.15 M. Excess natrophosphate was added to each solution to achieve saturation equilibrium at two different temperatures, 20°C and 36 °C. Once equilibrium was reached, the solutions were filtered, and the dissolved phosphorous (P) concentrations were determined using ICP-OES.

Figure 1 shows the concentration of P attributed to natrophosphate dissolution in solution vs. the added salt concentration, either NaF or $Na_3PO_4{\cdot}0.167NaOH{\cdot}12H_2O$. The data points for 0 M NaF and 0 M $Na_3PO_4{\cdot}0.167NaOH{\cdot}12H_2O$ are for the solubility of natrophosphate in 3.8 M $NaNO_3$ at 20 °C and 36 °C. The concentrations in solution are corrected to account for the initial amount of $Na_3PO_4{\cdot}0.167NaOH{\cdot}12H_2O$ present. The data revealed distinct solubility trends in response to the electrolyte composition. Natrophosphate exhibited higher solubility in NaF-containing solutions compared to those containing $Na_3PO_4{\cdot}0.167NaOH{\cdot}12H_2O$ and $NaNO_3$. At 20 °C, almost no natrophosphate dissolved in the $Na_3PO_4{\cdot}0.167NaOH{\cdot}12H_2O$ solutions as shown in Figure 1B and Figure 1D, indicating very low solubility under these conditions.

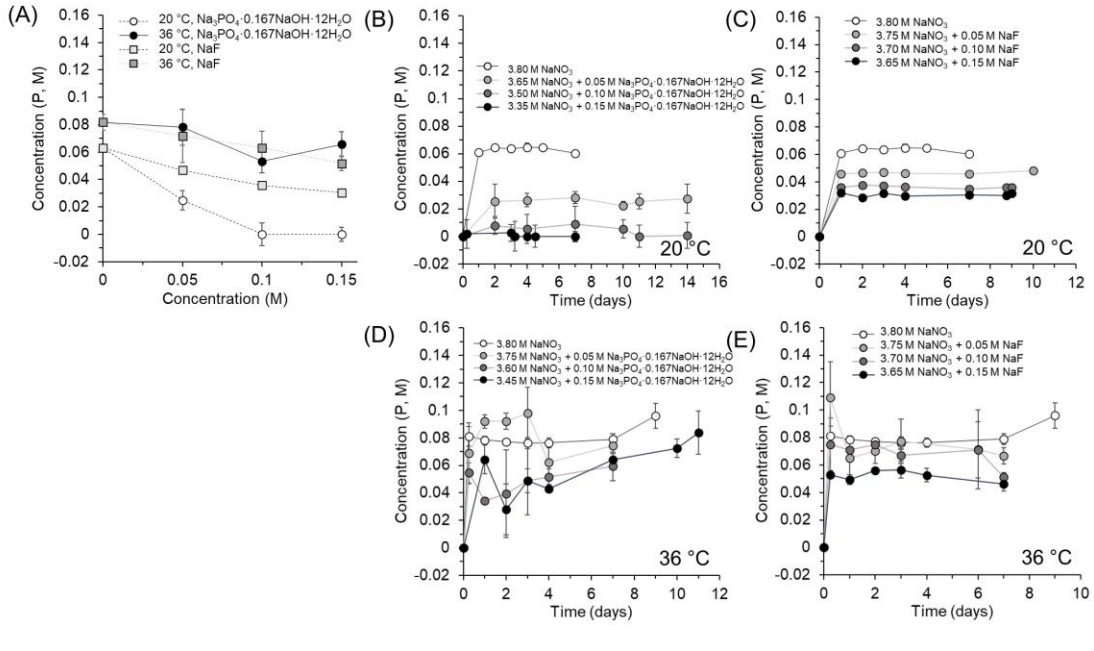

Figure 1. (A) Solubility of natrophosphate in 3.8 M Na composed of NaF and $NaNO_3$ or $Na_3PO_4{\cdot}0.167NaOH{\cdot}12H_2O$ and $NaNO_3$. The concentration of NaF and $Na_3PO_4{\cdot}0.167NaOH{\cdot}12H_2O$ is plotted on the x-axis. Time series tracking the dissolution of natrophosphate in (B) $Na_3PO_4{\cdot}0.167NaOH{\cdot}12H_2O$ and $NaNO_3$ at 20 °C, (C) NaF and $NaNO_3$ at 20 °C, (D) $Na_3PO_4{\cdot}0.167NaOH{\cdot}12H_2O$ and $NaNO_3$ at 36 °C, and (E) NaF and $NaNO_3$ at 20 °C.

In addition, the solution in which 0.15 M $Na_3PO_4{\cdot}0.167NaOH{\cdot}12H_2O$ solutions as was added to 3.35 M $NaNO_3$ did not fully dissolve prior to addition of natrophosphate. In that case, the

solution was filtered, natrophosphate was added, and negligible amounts of phosphorus was observed in solution. However, increasing the temperature to 36 °C enhanced solubility in these solutions, such that it was comparable and nearly equivalent to the solubility observed in NaF and $NaNO_3$ solutions.

In the time-dependent data, although complex due to overlapping conditions, provided valuable insights into the kinetics of solubility. The concentration of dissolved P was monitored over time, with sampling approximately once a day until equilibrium was reached, defined as the plateauing of the concentration values for at least three successive measurements. Equilibrium was generally reached within a few days for most conditions. This indicates that the system's approach to equilibrium is relatively rapid, irrespective of the initial composition.

The results indicate that the presence of both NaF and $NaNO_3$ reduces natrophosphate solubility at 20 °C. At the higher temperature of 36 °C, solubility increases, especially in solutions containing $Na_3PO_4{\cdot}0.167NaOH{\cdot}12H_2O$ and $NaNO_3$. Natrophosphate solubility in either NaF- or $Na_3PO_4{\cdot}0.167NaOH{\cdot}12H_2O$ containing solutions is only slightly less than natrophosphate solubility in $NaNO_3$ solutions at 36 °C.

Following the initial experiments, the solubility of natrophosphate was determined in solutions of NaX, where X represented various anions. The anions were Cl^-, OH^-, NO_3^-, NO_2^-, a mixture of CO_3 and NO_3. The solubility was also measured in water as a control, and Each solution was prepared with a fixed Na concentration, and excess natrophosphate was added to achieve saturation at equilibrium. The experiments were conducted at controlled temperatures, and the solutions were filtered post-equilibrium to determine the dissolved P concentration.

Figure 2A shows the final solubility concentration of P vs. different counterions, while the time-dependent data in Figure 2B and C show that equilibrium was reached over a period of several days. The results indicate that the presence of different counterions decreased the solubility of natrophosphate relative to water. In all cases, solutions containing Cl^-, OH^-, NO_3^-, NO_2^-, and CO_3^{2-} reduced the solubility of natrophosphate to ≤ 0.1 M, suggesting that the increase in ionic strength, or Na^+ concentration, is the dominant factor, rather than the nature of the counterion. However, the nature of the counterion does have some influence, with OH- having the greatest effect and CO_3^{2-} + NO_3^- having the least (Figure 2A). Note that there is also a slight reordering of the solubility of natrophosphate when comparing 20 and 36 °C. At 20 °C, the order is water > Na_2CO_3 +$NaNO_3$ > $NaNO_3$ > $NaNO_2$ = NaCl > NaOH, and at 35 °C, the order is water > Na_2CO_3 + $NaNO_3$ > NaCl > $NaNO_3$ > $NaNO_2$ = NaOH, with the placement of the NaCl system in the series being the most temperature significant.

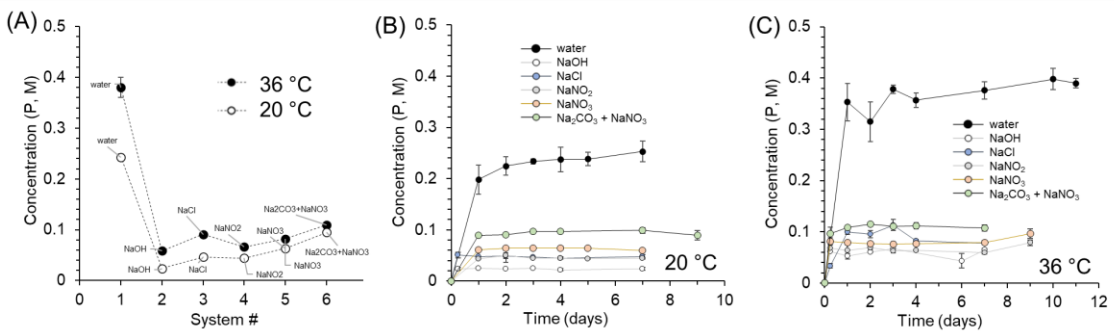

Figure 2. (A) Final solubility concentration of natrophosphate vs. various counterions (Cl^-, OH^-, NO_3^-, NO_2^-, carbonate, and water control). Time-dependent dissolution of natrophosphate at (B) 20 °C and (C) 36 °C.

The solubility of natrophosphate solids and, separately, gibbsite solids in a multicomponent simulant representative of waste from the southeast quadrant of the Hanford Site (Table 1**)** was then determined. Gibbsite solubility was also measured in the simulant supplemented with additional NaOH up to 3.8M. Upon preparation of the 3.8 M simulant at 20°C, the 3.8 M simulant with added NaOH at 20°C, and the 3.8 M simulant with added NaOH at 40 °C, precipitation was observed prior to natrophosphate and gibbsite. While a portion of the ion chromatography results are still undergoing analysis, a comparison of the available target and actual concentrations, shown in Table A5 – A6 in the Appendix, indicated that the sodium and fluoride concentrations were about 0.7 M less than expected, suggesting that a salt such as sodium fluoride potentially precipitated. Further solid-state characterization is underway to confirm the identity of the precipitate.

Figure 3A and D show aluminum (Al) concentration in solution as a function of NaOH concentration, and Figure 3B and C and Figure 3E and F show Al concentration in solution over time, both in the simulant and in the simulant with added NaOH. The data indicate that while the solubility of Al increases with increasing NaOH concentration, the rate of increasing solubility decreases at higher NaOH concentrations. The diminishing return of the progressive NaOH additions is more prominent at 20 °C than at 36 °C. The time-dependent data show that equilibrium solubility is typically reached within a few days under these experimental conditions.

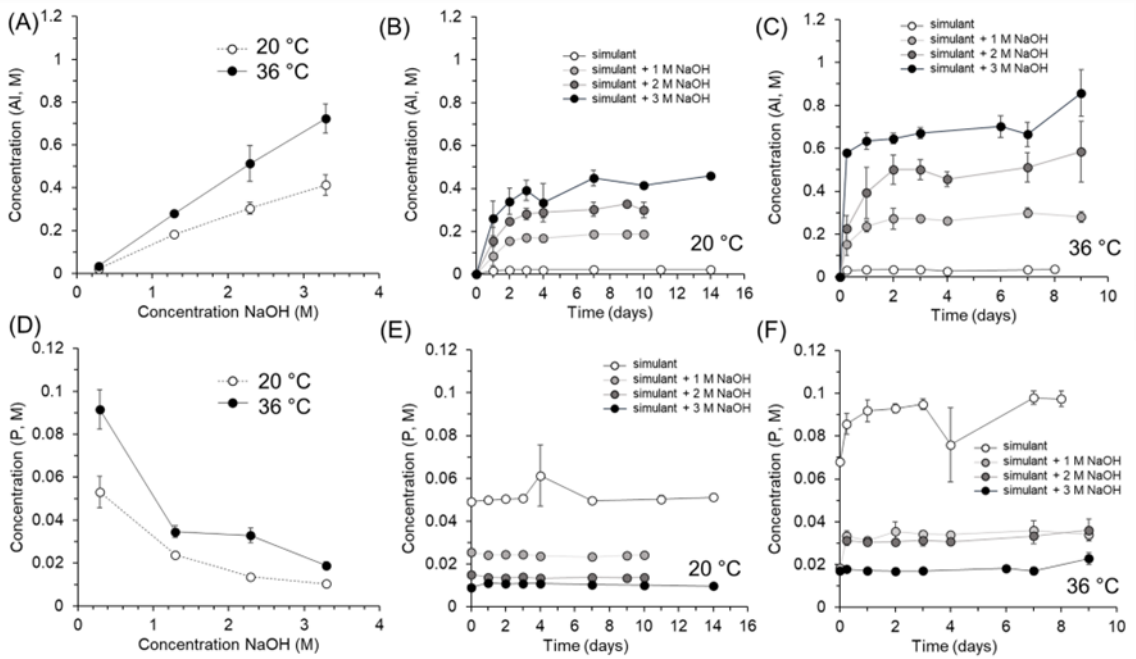

Figure 3. (A) Final solubility concentrations of Al with varying NaOH concentrations. Time-dependent data showing Al concentrations in solution for gibbsite in the presence of simulant and simulant with added NaOH at (B) 20 °C and (C) 36°C. (D) Final solubility concentrations of P with varying NaOH concentrations. Time-dependent data showing P concentrations in solution for gibbsite dissolution in the presence of simulant and simulant with added NaOH at (E) 20 °C and (F) 36°C.

Gibbsite solubility increased at the higher temperature, and with the addition of NaOH. However, the concentration of phosphate in solution decreased with NaOH addition, leading to precipitation of a new phase as gibbsite began to dissolve, indicating complex interactions between gibbsite dissolution and phosphate precipitation. These findings confirm that increased NaOH concentrations enhance gibbsite solubility but decrease phosphate solubility. Solid phase characterization will be conducted in Year 2 to identify the different phases of the precipitate as a function of solution composition.

Natrophosphate solubility in the presence of the simulant was also measured, as shown in Figure 4. At 36 °C, the solubility of natrophosphate was ~0.1 M in the simulant, and this decreased to a value of 0.07 M at 20 °C. Dilution of the solution saturated at 20 °C did result in appreciable precipitation. Comparison of these values with the studies in which the counterion of sodium salts was varied indicated the natrophosphate in the simulant has a higher solubility than binary systems composed of water and 3.8 M NaOH, $NaNO_2$, $NaNO_3$, and NaCl. The solubility of natrophosphate in the simulant is nearly equivalent to that in the Na_2CO_3 (0.5 M) and $NaNO_3$ (2.8 M) solution at 36 °C, whereas at 20 °C, the solubility of natrophosphate was greater in the Na_2CO_3 (0.5 M) and $NaNO_3$ (2.8 M) solution than in the simulant. In all cases, the solubility of natrophosphate is much greater in water.

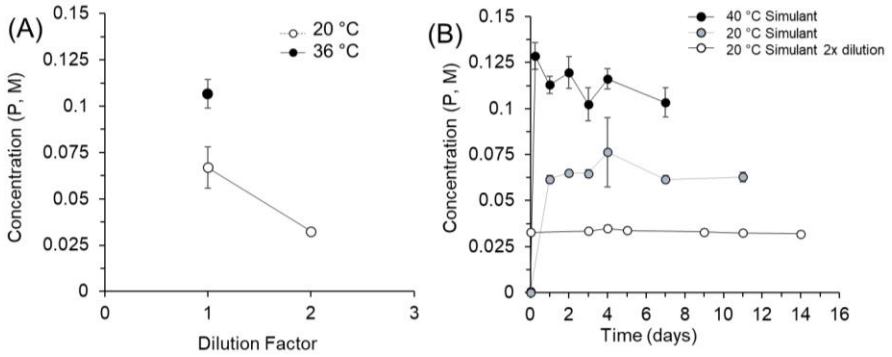

Figure 4. (A) Phosphorus (P) concentrations in simulant saturated with natrophosphate at 20 and 36 °C, and following dilution by a factor of 2 of the solution saturated with natrophosphate at 20 °C. (B) Time-dependent data showing P concentrations in solution for natrophosphate dissolution at 20 and 36 °C, and following dilution by a factor of 2 of the solution saturated with natrophosphate at 20 °C.

Table 2. Summary of natrophosphate solubility.

System	40 °C Conc. (M)	40 °C Conc. St. Dev. (M)	20 °C Conc. (M)	20 °C Conc. St. Dev. (M)
Water	0.380	0.016	0.243	0.020
3.8 M NaOH	0.059	0.009	0.024	0.002
3.8 M NaCl	0.091	0.006	0.046	0.002
3.8 M $NaNO_2$	0.066	0.004	0.044	0.001
3.8 M $NaNO_3$	0.082	0.006	0.063	0.002
3.8 M (Na_2CO_3 + $NaNO_3$)	0.110	0.005	0.095	0.006
Simulant	0.107	0.008	0.067	0.011

A series of tests were conducted to understand the impact of diluting the 3.8 Na simulant with deionized water on the solubility of aluminum and phosphorous. Figure 5 illustrates these trends for Al and P, along with the time-dependent data. The supernatant from equilibrated systems was filtered and diluted with water by factors of 2 and 4. The goal was to assess how changes in ionic strength and concentration affect solubility and potential precipitation. The results showed precipitation of Al post equilibration upon dilution, whereas the amount of phosphorus in solution remained constant upon dilution.

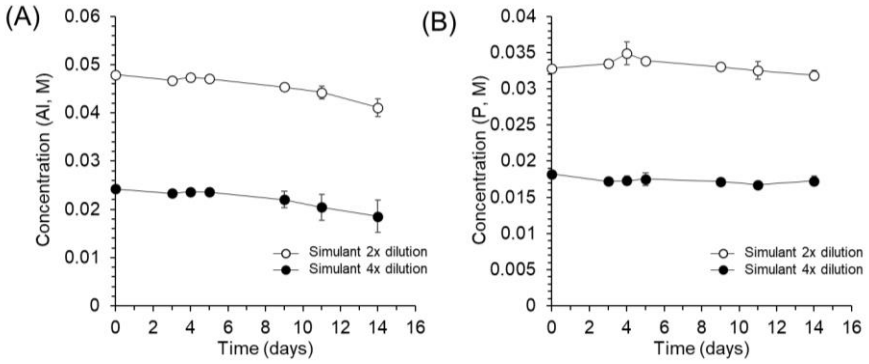

Figure 5. (A) Aluminum (Al) concentrations in 3.8 M Na simulant saturated with gibbsite before and after dilution by factors of 2 and 4. (B) Phosphorus (P) concentrations in 3.8 M Na simulant saturated with gibbsite before and after dilution by factors of 2 and 4.

7.0 Computational Chemistry Results

In addition to the experimental solubility studies, molecular dynamics simulations were employed to provide theoretical insights into the interactions between ions in the multicomponent electrolyte systems.

A 70% charge scaling was necessary during force field parameterization to reduce the excessive, concentration-dependent aggregation observed with full charges (Figure 6) and to produce diffusion coefficients more consistent with experimental values. With this scaling, the M2019 force field overestimates phosphorus diffusion at low concentrations, underestimates it at high concentrations, and consistently overestimates sodium diffusion across all concentrations (Figure 7A and B). In contrast, the Madrid Transport (MT) force field, while also underestimating both phosphorus and sodium diffusion at high concentrations, provides better overall agreement with experimental data.

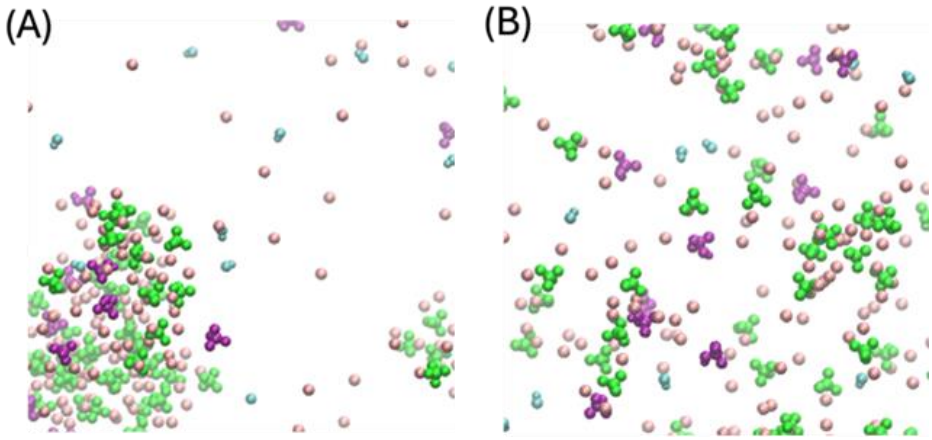

Figure 6. (A) Illustration of excessive $NaPO_4$ aggregation at 0.4 m using the M2019 force field, which has 85% charge scaling. (B) The clustering observed with the 70% charge scaled variant of M2019.

The phosphorus-sodium radial distribution functions in Figure 7C highlights structural differences that help explain the variation in predicted diffusion coefficients. In the M2019 force field, sodium exhibits bidentate interactions with phosphate at shorter distances than monodentate ones, potentially leading to overestimated sodium diffusion due to the faster motion of more compact ion pairs. In contrast, the MT force field shows only monodentate interactions and predicts lower diffusion coefficients. To better capture the mono-/bidentate interaction ratios and refine diffusion behavior, a series of Lennard-Jones parameter scalings were performed, following the original Madrid force field development approach. Because the phosphate ions were adopted from a different force field family, these interactions had not previously been fine-tuned. Initially, both ε and σ values were altered, however we found that scaling the σ by 7% (up for M2019 and down for MT) yielded substantial improvement by creating more similar binding preferences, and as such D values, for the two force fields. This further supports the claim of denticity having a direct relation with diffusion in solution. The final ratio of bidentate over monodentate interactions, being between 0.05 and 0.1, seems to generate the best matching diffusion coefficients through the concentration range. For both force fields, the decrease of this ratio is observed, and the amount of monodentate interaction increases as concentration increases.

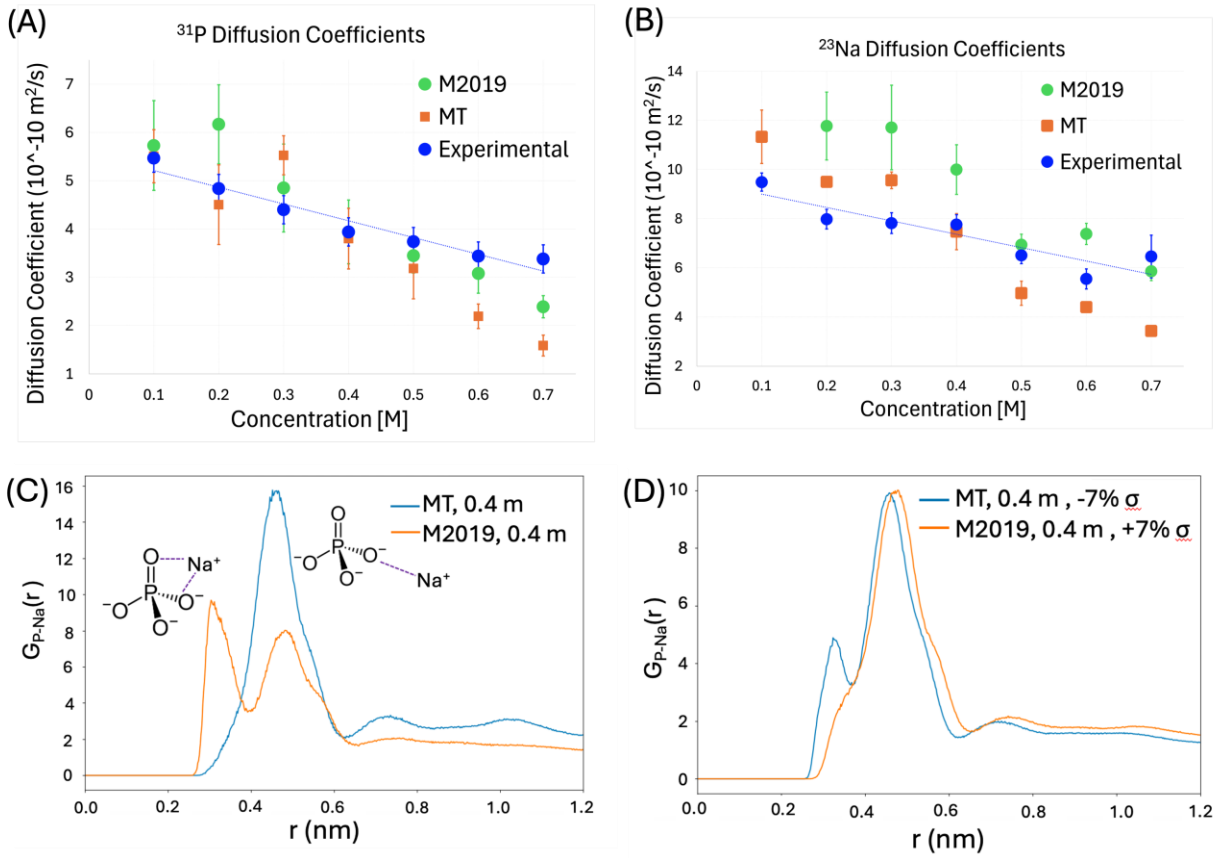

Figure 7. Ensemble averages of calculated diffusion coefficients of for (A) phosphorous and (B) sodium in solution produced from the final versions of the parametrized force fields with 70\% charge scaling and 7% σ increase for M2019 and decrease for MT. Radial distribution functions between P and Na in 0.4-m solution with MT and M2019 force fields at (C) 70\% charge scaling (D) 70\% charge scaling and 7\% σ scaling.

Ongoing work using CMD is analyzing the concentration and temperature-dependent clustering behavior of the $NaPO_4$ solutions. Of particular interest is the sensitivity of the diffusion coefficients to specific clustering ensembles. This is important as we move to more complex electrolyte solutions, where the introduction of new ions can alter the clustering behavior and provide deeper insights into the changes in solubility and solution transport properties due to ion aggregation and particle formation.

Complementing the CMD are AIMD studies of the local speciation preferences and reactivity of Na_3PO_4(aq), shown in Figure 8**.** First, we examined the energetic preferences for monodentate vs. bidentate coordination of P to Na using potential of mean force (PMF), wherein the mono-dentate configuration is preferred by 5.6 kcal/mol. Next, PMF simulations explored the energetic preferences of contact ion pair (CIP) vs. solvent separated ion pair (SSIP) configurations. In this case, we observed significant sensitivity of the potential energy surface to the specific constraints employed within the simulation. The sodium configurations about the anion dramatically influence both the reactivity of the anion as well as water that is in the first solvation and act as a proton source. As shown in Figure 8, for phosphate-phosphate interactions, two minima are observed. The shorter-distance phosphate dimer has two Na^+ bridging in a contact ion pair configuration, while the longer-distance dimer has one Na^+ bridging as a CIP and a

second Na^+ as an SSIP. Although we could not extend our simulations to longer distances, we believe a third minima will occur with both Na+ bridging in an SSIP configuration. The 2-CIP bridged species has a very similar configuration to the structure observed in the anhydrous sodium phosphate crystal structure, while a 2-SSIP bridged configuration would be most similar to the sodium phosphate dodecahydrate crystal structure.

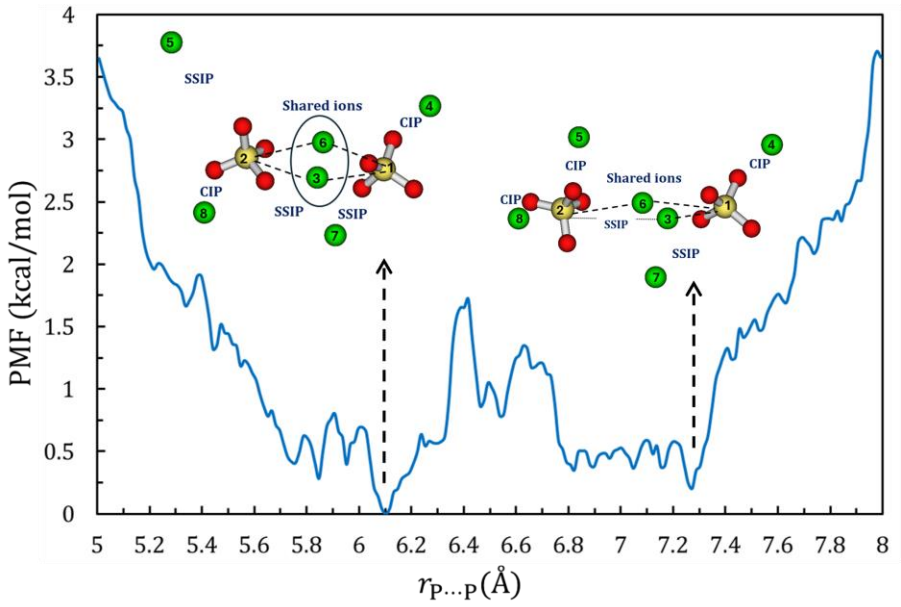

Figure 8. Potential of mean force for phosphate-phosphate interactions from AIMD simulations.

8.0 Conclusions

The primary goal of this work is to accelerate the overall mission schedule by enabling Direct Feed High-Level Waste (DFHLW) by remediating slurry properties from the SE quadrant. There is a significant amount of insoluble phosphate and fluoride in SE quadrant tank waste in the form of natrophosphate ($Na_7FPO_4 \cdot 19H_2O$). This study has greatly expanded our understanding of the solubility of natrophosphate and other tank waste materials (gibbsite ($Al(OH)_3$) and trisodium phosphate (Na_3PO_4)) in complex tank waste matrices that contain sodium salts of hydroxide (OH^-), phosphate (PO_4^{3-}), fluoride (F^-), nitrate (NO_3^-), nitrite (NO_2^-), and aluminate ($Al(OH)_4^-$). The results provide a pathway to enhance natrophosphate solubility by increasing temperature and adjusting electrolyte composition to maximize the amount of phosphate in solution while limiting the amount of washing and maintaining a high sodium molarity. The solubility data generated in this task also provide information on how natrophosphate and gibbsite solubility will change as a function of electrolyte composition and temperature:

- Natrophosphate exhibited higher solubility in NaF-containing solutions compared to $Na_3PO_4 \cdot 0.17NaOH \cdot 12H_2O$ and $NaNO_3$. At 20°C, very little phosphorous was soluble in $Na_3PO_4 \cdot 0.17NaOH \cdot 12H_2O$ solutions but increasing the temperature to 36°C enhanced solubility across all systems, demonstrating the influence of temperature on solubility dynamics.

- The nature of the anion had a strong effect on natrophosphate solubility. Natrophosphate solubility was highest in water and decreased in the presence of anions (Cl^-, OH^-, NO_3^-, NO_2^-). At 20°C, solubility decreased in the following order: water > Na_2CO_3 + $NaNO_3$ > $NaNO_3$ > $NaNO_2$ = NaCl > NaOH, whereas at 36°C, the order changed to water > Na_2CO_3 + $NaNO_3$ > NaCl > $NaNO_3$ > $NaNO_2$ = NaOH, indicating temperature-dependent solubility variations. At both temperatures tested, natrophosphate solubility was higher in the presence of CO_2^{3-}, and OH^- resulted in the lowest solubility

- For gibbsite in 3.8 M simulant, solubility increased with both temperature and NaOH concentration. However, phosphate concentrations in the simulant decreased with NaOH concentration, leading to the formation of precipitates and indicating complex interactions between gibbsite and phosphate in the presence of sodium hydroxide.

- When the 3.8 M Na simulant was diluted with water, the concentration of aluminum in solution decreased whereas phosphorus concentration remained constant, demonstrating the impact of dilution on precipitation behavior of gibbsite and phosphate.

- AIMD studies of sodium-phosphate interactions at dilute concentrations indicate an energetic preference for monodentate binding, facilitating Na^+ bridging of phosphate anions. Complementary CMD studies have developed a new sodium phosphate force field that accurately captures concentration-dependent diffusion coefficients of P and Na. Diffusion is highly sensitive to sodium binding modes to phosphate. Ongoing work focuses on how larger-scale aggregation of sodium phosphate clusters affects diffusion and precipitation.

In summary, for the transport of high aluminum waste containing gibbsite, a higher temperature of 36°C and a high concentration of NaOH are the optimum conditions to enhance gibbsite solubility and prevent precipitation. For high phosphate waste containing natrophosphate, a

higher temperature of 36°C is also optimal, but the solubility of natrophosphate is reduced in solutions containing NaOH.

Building on the results presented here, and in Task 2 (In-Tank Processing Using Low Temperature Aluminum Dissolution), in the next project year tests will be conducted to determine the ideal temperature and compositional conditions for effective sludge retrieval to provide a stable solution (no gelation or precipitation) with carrier fluid density suitable for waste transport. The data generated will be used to produce an empirical model of anion effects on natrophosphate solubility. Once the ideal temperature and compositional conditions have been identified, they will be used in cesium ion exchange column, batch contact, and evaporator testing in Task 5 (Leachate Disposition) to confirm that the sludge washing leachate can be disposed of effectively. Molecular dynamics simulations will be employed to correlate solution composition with ion interactions, enhancing the understanding of solubility behavior at a molecular level. Future studies will validate these findings using actual waste samples from the Hanford Site. Solubility measurements will also be extended to include interactions with clarkeite and zirconia, providing insights into the behavior of uranium and zirconium in waste solutions.

9.0 References

Britton, M. D. 2019a. *Solubility Data Review*. RPP-RPT-60326, Rev. 3, Washington River Protection Solutions LLC, Richland, WA.

Britton, M. D. 2019b. *Analysis of GCALC Solubility Prediction Accuracy Between Rev 0 and Rev 2 Parameters*. RPP-RPT-61498, Rev. 0, Washington River Protection Solutions, Richland, WA.

Colburn, H. A., and R. A. Peterson. 2021. “A history of Hanford tank waste, implications for waste treatment, and disposal.” *Environmental Progress & Sustainable Energy* 40:e13567. https://doi.org/10.1002/ep.13567

Delegard CH, CI Pearce, and MS Fountain. 2018. *Precipitation Risk when Diluting DFLAW Feed Saturated in Aluminum Hydroxide*. PNNL-27312, RPT-OSIF-002, Rev. 0, Pacific Northwest National Laboratory, Richland, Washington.

Dembowski, M., M. M. Snyder, C. H. Delegard, J. G. Reynolds, T. R. Graham, H.-W. Wang, I. I. Leavy, S. R. Baum, O. Qafoku, M. S. Fountain, K. M. Rosso, S. B. Clark, and C. I. Pearce. 2020. “Ion-ion interactions enhance aluminum solubility in alkaline suspensions of nanogibbsite (α-$Al(OH)_3$) with sodium nitrite/nitrate.” *Physical Chemistry Chemical Physics* 22(8):4368-4378. https://doi.org/10.1039/C9CP05856G

Graham, T. R., E. T. Nienhuis, J. G. Reynolds, J. Marcial, J. S. Loring, K. M. Rosso, and C. I. Pearce. 2022. “Sodium site occupancy and phosphate speciation in natrophosphate are invariant to changes in NaF and Na_3PO_4 concentration." *Inorganic Chemistry Frontiers* 9:4864-4875. https://doi.org/10.1039/D2QI00868H

Jordan, E. L. 2022. *Final Analytical Report for Tank 241-AN-106 Core 2020-10 Sampling and Analysis Plan*. RPP-RPT-63779, Washington River Protection Solutions, Inc., Richland, WA.

Miller, F. G., and M. D. Britton. 2017. *Analysis of GCALC Solubility Prediction Accuracy for Reference Data*. RPP-RPT-60336, Washington River Protection Solutions, Richland, WA.

Misra C. 1970. “Solubility of aluminium trihydroxide (hydrargillite) in sodium hydroxide solutions.” *Chemistry and Industry* 19(5):619-623.

Westesen, A. M., A. M. Robb, N. L. Cappella, C. Alvarez, and R. A. Peterson. 2023. *Phosphate and Fluoride Processing Options for Hanford Sludge*. PNNL-34456, Rev. 0, Pacific Northwest National Laboratory, Richland, WA.

Zhang, X. (Xin), X. (Xianwen) Zhang, T. R. Graham, C. I. Pearce, B. L. Mehdi, A. Y. N'Diaye, S. Kerisit, N. D. Browning, S. B. Clark, and K. M. Rosso. 2017. “Fast Synthesis of Gibbsite Nanoplates and Process Optimization Using Box-Behnken Experimental Design.” *Crystal Growth & Design* 17:6801-6808.

Zhu, C., Gong, L., & Tie, S.-n. 2020. "Influence of preparation processes on thermophysical properties of molten salt." *AIP Advances*, 10(2), 025214. https://doi.org/10.1063/1.5129609

Appendix A

Table A.1. Compositions for natrophosphate solubility in NaF:Na_3PO_4:$NaNO_3$:H_2O with 3.8 M Na total

System #	Species in Excess	$Na_3PO_4 \cdot 0.167NaOH \cdot 12H_2O$ (M)	NaF (M)	$NaNO_3$ (M)
0	natrophosphate	0	0	0
1	natrophosphate	0.05	0	3.65
2	natrophosphate	0.10	0	3.50
3	natrophosphate	0.15	0	3.35
4	natrophosphate	0	0.05	3.75
5	natrophosphate	0	0.10	3.70
6	natrophosphate	0	0.15	3.65

Table A.2. Compositions for natrophosphate solubility in 3.8 M NaX solutions

System #	Species in Excess	Make up to 3.8 M Na using
7	natrophosphate	NaOH
8	natrophosphate	NaCl
9	natrophosphate	$NaNO_2$
10	natrophosphate	$NaNO_3$
11	natrophosphate	Na_2CO_3 (0.5 M) and $NaNO_3$ (2.8 M)

Table A.3. Compositions for natrophosphate solubility in 3.8 M Na simulant, gibbsite solubility in 3.8 M Na simulant, and gibbsite solubility in simulants amended with NaOH.

System #	Species in Excess	Na_3PO_4	NaF	NaOH	$NaAlO_2$	Na_2CO_3	KCl	$NaNO_2$	$NaNO_3$
12	natrophosphate	0	0	C_{sim}	C_{sim}	C_{sim}	C_{sim}	C_{sim}	C_{sim}
13	gibbsite	C_{sim}	C_{sim}	C_{sim}	0	C_{sim}	C_{sim}	C_{sim}	C_{sim}
14	gibbsite	C_{sim}	C_{sim}	1.8 M	0	C_{sim}	C_{sim}	C_{sim}	C_{sim}
15	gibbsite	C_{sim}	C_{sim}	2.8 M	0	C_{sim}	C_{sim}	C_{sim}	C_{sim}
16	gibbsite	C_{sim}	C_{sim}	3.8 M	0	C_{sim}	C_{sim}	C_{sim}	C_{sim}

Table A.4. A dilution series of the high Na simulant is shown.

System #	Dilution Factor
12-1	2
12-2	4
16-1	2
16-2	4

Table A.5. Target and actual concentrations before addition of natrophosphate (S0-S12) or gibbsite (S14-S16), in addition to initial concentrations following dilution (S12-1, S12-2, S16-1, and S16-2) The concentrations are in units of M (mol/L). Values pending analysis are marked as "-".

Bulk Solutions			Na (ICP)		P (ICP)		Al (ICP)		NO_2 (IC)	
Sample ID	System	Temp	Est Conc	Act Conc	Est Conc	Act Conc	Est Conc	Act Conc	Est Conc	Act Conc
S0 - 20C	0	20	0	0.09	0	0	0	0	0	0.01
S1 - 20C	1	20	3.8	4.03	0.05	0.04	0	0	0	0
S2 - 20C	2	20	3.8	4.19	0.1	0.09	0	0	0	0
S3 - 20C	3	20	3.8	4.07	0.15	0.12	0	0	0	-
S4 - 20C	4	20	3.8	4.07	0	0	0	0	0	0
S5 - 20C	5	20	3.8	3.97	0	0	0	0	0	0
S6 - 20C	6	20	3.8	3.88	0	0	0	0	0	0
S7 - 20C	7	20	3.8	4.3	0	0	0	0	0	0
S8 - 20C	8	20	3.8	3.84	0	0	0	0	0	0
S9 - 20C	9	20	3.8	4.13	0	0	0	0	3.8	-
S10 - 20C	10	20	3.8	3.96	0	0	0	0	0	0.01
S11 - 20C	11	20	3.8	3.27	0	0	0	0	0	0
S12 - 20C	12	20	4.15	3.36	0	0	0.09	0.09	1.06	1.35
S12-1 - 20C	1-Dec	20	N/A	1.8	N/A	0.03	N/A	0.05	N/A	0.58
S12-2 - 20C	2-Dec	20	N/A	0.84	N/A	0.02	N/A	0.02	N/A	0.27
S13 - 20C	13	20	4.33	3.8	0.09	0.05	0	0	1.06	1.16
S14 - 20C	14	20	5.84	5.6	0.09	0.03	0	0	1.06	-
S15 - 20C	15	20	6.84	6.93	0.09	0.02	0	0	1.06	-
S16 - 20C	16	20	7.84	6.93	0.09	0.01	0	0	1.06	1.1
S16-1 - 20C	16-1	20	N/A	3.77	N/A	0	N/A	0.25	N/A	0.56
S16-2 - 20C	16-2	20	N/A	1.88	N/A	0	N/A	0.13	N/A	0.27
S0 - 40C	0	40	0	0.02	0	0	0	0	0	0
S1 - 40C	1	40	3.8	3.99	0.05	0.05	0	0	0	-
S2 - 40C	2	40	3.8	4.22	0.1	0.08	0	0	0	-
S3 - 40C	3	40	3.8	3.33	0.15	0.1	0	0	0	0
S4 - 40C	4	40	3.8	3.89	0	0	0	0	0	-
S5 - 40C	5	40	3.8	4.84	0	0	0	0	0	-
S6 - 40C	6	40	3.8	-	0	-	0	-	0	-
S7 - 40C	7	40	3.8	3.74	0	0	0	0	0	-
S8 - 40C	8	40	3.8	4.01	0	0	0	0	0	-
S9 - 40C	9	40	3.8	-	0	-	0	-	3.8	-
S10 - 40C	10	40	3.8	-	0	-	0	-	0	-
S11 - 40C	11	40	3.8	-	0	-	0	-	0	-
S12 - 40C	12	40	4.15	3.43	0	0	0.09	0.08	1.06	-
S13 - 40C	13	40	4.33	2.59	0.09	0.07	0	0	1.06	-
S14 - 40C	14	40	5.84	3.13	0.09	0.02	0	0	1.06	-
S15 - 40C	15	40	6.84	6.43	0.09	0.03	0	0	1.06	-
S16 - 40C	16	40	7.84	6.66	0.09	0.02	0	0	1.06	-

Table A.6. Target and actual concentrations before addition of natrophosphate (S0-S12) or gibbsite (S14-S16), in addition to initial concentrations following dilution (S12-1, S12-2, S16-1, and S16-2) The concentrations are in units of M (mol/L). Values pending analysis are marked as "-".

Bulk Solutions		NO_3 (IC)		F (IC)		Cl (IC)		CO_2 (Alkalinity)	
Sample ID	Temp	Est Conc	Act Conc	Est Conc	Act Conc	Est Conc	Act Conc	Est Conc	Act Conc
S0 - 20C	20	0	0	0	0	0	0	0	0.1
S1 - 20C	20	3.65	3.38	0	0	0	0	0	0.09
S2 - 20C	20	3.5	3.16	0	0	0	0	0	0.08
S3 - 20C	20	3.35	-	0	-	0	-	0	0.06
S4 - 20C	20	3.75	3.09	0.05	0.05	0	0	0	0.12
S5 - 20C	20	3.7	3.2	0.1	0.1	0	0	0	0.08
S6 - 20C	20	3.65	3.1	0.15	0.15	0	0	0	0.02
S7 - 20C	20	0	0	0	0	0	0	0	0.02
S8 - 20C	20	0	0	0	0	3.8	-	0	0.03
S9 - 20C	20	0	0.02	0	0	0	0	0	0.02
S10 - 20C	20	3.8	-	0	0	0	0	0	0.01
S11 - 20C	20	2.8	2.63	0	0	0	0	0.5	0.47
S12 - 20C	20	0.71	0.71	0.7	0	0.03	0.03	0.65	0.65
S12-1 - 20C	20	N/A	0.38	N/A	0.01	N/A	0.02	N/A	0.31
S12-2 - 20C	20	N/A	0.18	N/A	0.01	N/A	0.01	N/A	0.16
S13 - 20C	20	0.71	0.62	0.7	0.05	0.03	0.02	0.65	0.66
S14 - 20C	20	0.71	-	0.7	-	0.03	-	0.65	0.72
S15 - 20C	20	0.71	-	0.7	-	0.03	-	0.65	0.74
S16 - 20C	20	0.71	0.7	0.7	0.04	0.03	0.06	0.65	0.69
S16-1 - 20C	20	N/A	0.35	N/A	0.01	N/A	0.02	N/A	0.34
S16-2 - 20C	20	N/A	0.17	N/A	0	N/A	0.01	N/A	0.17
S0 - 40C	40	0	0.01	0	0	0	0	0	0.06
S1 - 40C	40	3.65	-	0	-	0	-	0	0.09
S2 - 40C	40	3.5	-	0	-	0	-	0	0.09
S3 - 40C	40	3.35	2.63	0	0	0	0	0	0.08
S4 - 40C	40	3.75	-	0.05	-	0	-	0	0.12
S5 - 40C	40	3.7	-	0.1	-	0	-	0	0.14
S6 - 40C	40	3.65	-	0.15	-	0	-	0	0.16
S7 - 40C	40	0	-	0	-	0	-	0	0.12
S8 - 40C	40	0	-	0	-	3.8	-	0	0.1
S9 - 40C	40	0	-	0	-	0	-	0	0.12
S10 - 40C	40	3.8	-	0	-	0	-	0	0.12
S11 - 40C	40	2.8	-	0	-	0	-	0.5	0.63
S12 - 40C	40	0.71	-	0.7	-	0.03	-	0.65	0.71
S13 - 40C	40	0.71	-	0.7	-	0.03	-	0.65	0.67
S14 - 40C	40	0.71	-	0.7	-	0.03	-	0.65	0.71
S15 - 40C	40	0.71	-	0.7	-	0.03	-	0.65	0.72
S16 - 40C	40	0.71	-	0.7	-	0.03	-	0.65	0.75

Table A.7. Notes regarding solubilities acquired before addition of natrophosphate (S0-S12) or gibbsite (S14-S16), in addition to initial concentrations following dilution (S12-1, S12-2, S16-1, and S16-2) The concentrations are in units of M (mol/L). If the sample

Bulk Solutions		
Sample ID	Temp	Fully dissolved prior to solubility test
S0 - 20C	20	Yes
S1 - 20C	20	Yes
S2 - 20C	20	Yes
S3 - 20C	20	No
S4 - 20C	20	Yes
S5 - 20C	20	Yes
S6 - 20C	20	Yes
S7 - 20C	20	Yes
S8 - 20C	20	Yes
S9 - 20C	20	Yes
S10 - 20C	20	Yes
S11 - 20C	20	Yes
S12 - 20C	20	No
S12-1 - 20C	20	N/A
S12-2 - 20C	20	N/A
S13 - 20C	20	No
S14 - 20C	20	No
S15 - 20C	20	No
S16 - 20C	20	No
S16-1 - 20C	20	N/A
S16-2 - 20C	20	N/A
S0 - 40C	40	Yes
S1 - 40C	40	Yes
S2 - 40C	40	Yes
S3 - 40C	40	Yes
S4 - 40C	40	Yes
S5 - 40C	40	Yes
S6 - 40C	40	Yes
S7 - 40C	40	Yes
S8 - 40C	40	Yes
S9 - 40C	40	Yes
S10 - 40C	40	Yes
S11 - 40C	40	Yes
S12 - 40C	40	Yes
S13 - 40C	40	No
S14 - 40C	40	No
S15 - 40C	40	No
S16 - 40C	40	No

Table A.8. Solution characterization before addition of natrophosphate (S0-S12) or gibbsite (S14-S16), in addition to initial concentrations following dilution (S12-1, S12-2, S16-1, and S16-2) Values pending analysis are marked as "-".

System ##	pH initial	pH final	ρ initial (g/cm^3)	ρ final (g/cm^3)	Viscosity initial (cp)	Viscosity final (cp)
S0 - 20C	7.8	12.4	0.999	1.054	0.98	1.32
S1 - 20C	11.8	11.8	1.199	1.203	1.49	1.58
S2 - 20C	12.1	12.1	1.201	1.201	1.57	1.58
S3 - 20C	12.2	12.2	1.201	1.201	1.59	1.60
S4 - 20C	7.2	11.4	1.915	-	1.45	1.55
S5 - 20C	9.1	11.3	1.196	1.200	1.46	1.54
S6 - 20C	9.3	11.3	1.195	1.199	1.47	1.53
S7 - 20C	13.4	13.4	1.145	1.149	2.39	2.48
S8 - 20C	7.7	11.3	1.142	1.148	1.50	1.62
S9 - 20C	9.3	11.4	1.156	1.163	1.47	-
S10 - 20C	7.4	11.5	1.196	1.207	1.43	-
S11 - 20C	10.2	10.7	1.189	1.200	-	1.47
S12 - 20C	-	13.0	1.120	1.165	-	-
S12-1 - 20C	-	13.0	1.153	1.162	-	-
S12-2 - 20C	13.5	13.6	1.209	1.214	-	-
S13 - 20C	13.6	13.5	1.242	1.245	-	-
S14 - 20C	-	13.4	1.270	1.276	-	-
S15 - 20C	-	12.8	1.084	1.086	-	1.33
S16 - 20C	-	12.6	1.042	1.043	-	1.14
S16-1 - 20C	-	13.6	1.130	1.153	-	-
S16-2 - 20C	-	13.5	1.065	1.079	-	-
S0 - 40C	6.0	12.3	0.998	1.051	-	-
S1 - 40C	11.7	11.6	-	-	-	-
S2 - 40C	12.0	11.9	-	-	-	-
S3 - 40C	12.2	12.2	-	-	-	-
S4 - 40C	7.6	11.4	-	-	-	-
S5 - 40C	7.5	11.3	-	-	-	-
S6 - 40C	8.1	11.4	-	-	-	-
S7 - 40C	13.6	13.6	-	-	-	-
S8 - 40C	8.4	11.1	-	-	-	-
S9 - 40C	8.7	11.4	-	-	-	-
S10 - 40C	7.6	11.4	-	-	-	-
S11 - 40C	10.2	10.8	-	-	-	-
S12 - 40C	12.8	12.9	1.141	1.148	-	-
S13 - 40C	12.9	12.9	1.152	1.171	-	-
S14 - 40C	13.5	-	1.205	1.207	-	-
S15 - 40C	13.5	13.5	1.214	1.250	-	-
S16 - 40C	13.5	13.6	1.262	1.273	-	-

Pacific Northwest National Laboratory

902 Battelle Boulevard
P.O. Box 999
Richland, WA 99354

1-888-375-PNNL (7665)

www.pnnl.gov